Drying behavior of calcium silicate

Marnix Van Belleghem, Marijke Steeman, Arnold Janssens and Michel De Paepe

In: Journal of Construction and Building Materials, 65, pp. 507-517, 2014.

Drying behaviour of calcium silicate

M. Van Belleghem[1], M. Steeman[2], A. Janssens[3] and M. De Paepe[1]

[1] Ghent University, Department of Flow, Heat and Combustion Mechanics, Sint-Pietersnieuwstraat 40, B-9000 Gent, Belgium
[2] Ghent University, Department of Industrial Technologies and Construction, Research group Construction and Structural Engineering & Surveying, Valentin Vaerwijckweg 1, B-9000 Gent, Belgium
[3] Ghent University, Department of Architecture and Urban Planning, Jozef Plateaustraat 22, B-9000 Gent, Belgium

Corresponding author: Marnix Van Belleghem
Tel +3292643289 / Fax +3292643575
Email: marnix.vanbelleghem@UGent.be

Abstract

Nowadays, the hygrothermal performance of the building envelope is often evaluated using HAM (heat, air and moisture) models. These models can be used to predict the hygrothermal response of the building envelope and can assist in reducing the risk of any moisture-related damage (e.g. decrease of thermal insulation value due to wetting, interstitial condensation etc.). At the same time it is important to understand the physical mechanisms of wetting and drying of building materials. Experimental research can contribute to a better understanding of these mechanisms.
In this paper the focus lies on the wetting and drying phenomena occurring in building materials. One specific material is highlighted: calcium silicate. Calcium silicate is an inorganic, hygroscopic and capillary active insulation material, which is often used in interior thermal insulations systems. The paper describes a drying experiment in which a calcium silicate sample dries out starting from saturation. The experiments showed that calcium silicate has an atypical drying behaviour: during the second drying phase an intermediate plateau was observed in the temperature course. Numerical simulations performed with a recently developed CFD-HAM model were compared with the experimental results and were used to explain the experimental observations.

Nomenclature

C	Specific heat capacity [J/kgK]
C_b	Stefan-Boltzmann constant [W/m²K^4]
D_{va}	diffusivity of water vapour into air [m²/s]
E	Total energy [J/m³]
g	Moisture flux [kg/m²s]
h	Specific enthalpy [J/kg]
h	Convective heat transfer coefficient [W/m²K]
h_m	Convective mass transfer coefficient [s/m]
k	Turbulent kinetic energy [J]
K_l	Liquid permeability [s]
L	Latent heat of evaporation [J/kg]
p_c	capillary pressure [Pa]
p_{sat}	Saturation vapour pressure [Pa]
p_v	Partial vapour pressure [Pa]
q	Heat flux [W/m²]
RH	Relative humidity [-]
R_v	specific gas constant for water vapour [J/kgK]
t	Time [s]
T	Temperature [K]
w	moisture content [kg/m³]
$\partial w/\partial p_c$	Moisture capacity [kg/m³Pa]
y+	Dimensionless distance to the wall [-]
Greek symbols	
ε	Emissivity [-]

λ	Thermal conductivity [W/mK]
μ	Water vapour resistance factor [-]
ρ	Density [kg/m³]
ψ_0	Open porosity [-]
ω	Specific dissipation rate of turbulent kinetic energy [1/s]
Subscripts	
c	Capillary
l	Liquid
mat	Material
rad	Radiation
s	Surface
sat	Saturation
v	Vapour
Acronyms	
2D	2 dimensional
3D	3 dimensional
ACH	Air changes per hour
Al	Aluminium
CaSi	Calcium Silicate
CFD	Computational Fluid Dynamics
CRP	Constant drying rate period
FRP	Falling drying rate period
HAM	Heat, air and moisture transport model
PUR	Polyurethane
SIMPLE	Semi-implicit method for pressure linked equations
SST	Shear stress transport

1. Introduction

During the last decades, the requirements for buildings have increased tremendously: a comfortable indoor climate and a healthy environment are desired for the building occupants, in combination with a sustainable and energy efficient design and a low energy use.

Although the quality of building envelopes has grown during the last decades, moisture-related problems may still arise. Moisture-damage can be the result of rising damp, surface condensation (as a result of thermal bridges) or interstitial condensation (for instance caused by interior insulation systems). The presence of a high moisture content in building envelopes during service life should be avoided: an increased moisture content may lead to serious structural as well as to aesthetic problems: corrosion, loss of thermal insulation quality [1,2], mould and mildew [3], salt efflorescence [4,5] etc. Avoiding the risk of damage to the building envelope is related to the hygrothermal performance of building materials and building envelope systems. HAM (heat, air and moisture) models are widely used to predict heat and mass transfer in building envelope systems and allow building designers to evaluate the performance of the building and its envelope in advance or to suggest alternative solutions in case of deficiencies. The knowledge of the wetting and drying behaviour of building materials is an important aspect in this matter.

In the past a lot of research has been done on the drying and wetting kinetics of porous materials in general and on building materials in particular. A wide range of textbooks can be found that describe the combined heat and moisture transport in porous materials [6,7]. Based on this knowledge several numerical models have been developed that help scientists and engineers to study and predict drying and wetting of porous (building) materials.

The past decade the drying behaviour of the most common building materials has been studied with numerical models. Most of these materials are hygroscopic and/or capillary active (wood [8], gypsum board [9], brick [10-12]). Insulation materials on the other hand are one class of building materials that is seldom addressed in drying studies. This is because most insulation materials (XPS, EPS, PUR, PIR, mineral wool …) are non-hygroscopic and non-capillary active.

However some building materials with a fine pore structure combine a hygroscopic and capillary active behaviour with a low thermal conductivity. An example of such a material is calcium silicate.
Calcium silicate (Ca_2SiO_4) is an inorganic, hygroscopic and capillary active insulation material. It is composed of hydrous calcium silicate and reinforcing fibres. It is produced by autoclaving the slurry of lime and silica powder, adding some fibrous filler. The resulting mixture is formed into desired shapes [13]. Due to its resistance to high temperatures it is often used as high-temperature or fire resistant insulation. It is also often used as thermal insulation material in interior thermal insulation systems without water vapour barrier, e.g. in historic buildings where the original façade must be kept in its original appearance [14].
The high moisture buffering capacity of the material enables it to dampen humidity variations and occasional interstitial condensation can be redistributed and transported out of the material due to the high capillary activity [15]. The material has a higher capillary moisture content than for example brick. The pore volume distribution of calcium silicate is characterized by a broad pore system including a significant fraction of fine pores in the hygroscopic region and a coarse pore system in the capillary region [16]. The pore size varies from several nanometers up to a millimeter [13].

Researchers have already been working on the characteristics of the calcium silicate material. For example Hamilton and Hall have studied its chemical and mineralogical composition [17]. The relationships between thermal conductivity and microstructural parameters, such as porosity and pore size were experimentally studied by Do et al. for two calcium silicate boards of different densities [18]. Mar et al. developed a theoretical model for the thermal conductivity and apparent thermal conductivity of calcium silicate for a wide range of temperature and moisture conditions [13].
The hygric properties of calcium silicate (capillary moisture uptake, absorption coefficient, isothermal adsorption and desorption curves, water vapour resistance factor), have been extensively measured by six laboratories in the frame of the HAMSTAD project [19]. More recently, Pavlík et al. measured moisture profiles in desorption in a calcium silicate sample using time domain reflectometry. The results were used as input data for determining the moisture diffusivity of the material during drying [14]. Pease et al. used X-ray attenuation measurements to monitor the moisture content of building materials, amongst others calcium silicate [20]. The influence of the relative humidity on the diffusion process of VOC's in porous materials was studied by Xu et al. [21].
Due to its hygroscopic and capillary characteristics, calcium silicate is also often used in heat and mass transfer experiments to validate HAM models. In the past, it has been used to validate a coupled CFD-HAM model and a coupled BES-HAM model [22-25].
In this paper however the drying behaviour of calcium silicate when initially saturated with water is studied. Due to the combination of a high capillary activity and low thermal conductivity when dry, the drying behaviour of the material deviates from that of other porous building materials such as wood, brick etc.
First the experimental setup, used for the convective drying experiment, is described. Temperature and mass change were monitored and are discussed. Next the experiment is modelled with a recently developed heat and moisture transport model. This comparison helps in explaining the observed drying behaviour.

2. Calcium silicate drying experiment

2.1. Experimental setup

A sample of calcium silicate was saturated with water and placed in a climate chamber. The test sample measures 10cm x 10cm x 5cm. The sides and bottom of the sample were sealed for moisture by silicone rubber. Polyurethane foam with a thickness of 5cm and thermal conductivity of 0.023 W/mK was used as insulation for the sample sides. The top of the sample was exposed to a conditioned air flow. Figure 1 shows the location of the sample in the climate chamber. A detailed description of the climate chamber can be found in [22-23]. The sample was installed in the climate chamber just beneath the chamber air inlet on a balance. In this position, the air jet flows just over the top surface of the sample.

A climate chamber is used to ensure well-controlled boundary conditions. The test facility was built at the laboratory of the Department of Flow, Heat and Combustion Mechanics at Ghent University (www.floheacom.ugent.be) and consists of an outer chamber (3.0m width x 2.7m depth x 2.4m height) and an inner chamber which is the actual test chamber (1.8m width x 1.89m depth x 1.8m width). Both the outer and inner room are well-insulated and the inner room is vapour tight.
Using this chamber and the accompanying air handling unit, it is possible to control the supply air velocity, temperature and relative humidity. During these experiments, the inlet air temperature was controlled at 30 ± 0.1°C, the relative humidity of the inlet air was 20 ± 1.4%. The test room was ventilated with an air change rate of 10ACH.

Temperature and relative humidity at various depths in the sample and mass evolution were monitored over time during the drying of the sample. Thermocouples were inserted in the calcium silicate sample by drilling small holes in order to monitor the drying experiment. Figure 2 shows a schematic representation of the test sample and the location of the different thermocouples. Six thermocouples were inserted in the calcium silicate sample, one row of three thermocouples was installed at 7mm depth in the sample, the second row of three thermocouples was placed at 17mm. In each row, one thermocouple was installed centrally in the sample, the two others were installed respectively upstream and downstream of this thermocouple. The aim was to evaluate whether the inlet airflow has an influence on the drying rate at different positions in the sample.

An extra thermocouple was installed at the bottom of the sample and finally the last thermocouple was inserted in the bottom insulation. Temperature is measured with an accuracy of 0.1°C after calibration.
At the same time the mass change of the test setup is measured by a precision balance (PE1200 Mettler-Toledo). After calibration the precision of the balance was estimated at 2g. The size of the test sample was large enough so that the total mass change during drying could be measured with a sufficient accuracy. The total mass of the test setup with saturated sample is ± 1200g resulting in a relative uncertainty of 0.16%. The relative uncertainty increases to 0.25% when the sample is dry. The total mass loss during the experiment was 388g. When this is used as a reference for the relative uncertainty this uncertainty would be 0.5%.

2.2. Velocity profile

A 2D hotwire anemometer was used to measure the velocity profile near the climate chamber inlet. The air inlet had a round section, with a diameter of 5 cm. The anemometer was connected to a robot arm which was controlled by a computer. The robot arm could move in two directions, allowing measurements in the vertical cross-plane of the jet. Since the inlet of the chamber could be assumed symmetrical, only half of the inlet was measured. Figure 3 shows the results of the air velocity measured in front of the air inlet. In the figure the vertical velocity distribution just in front of the air inlet is shown. For symmetry reasons, only half of the velocity profile was measured. The measurements at each location were performed during a sufficiently long time to reach convergence. The air velocity at the centre of the inlet was around 14 m/s. The average turbulent intensity measured at the inlet was 3%.

2.3. Limitations of the measurement setup

The described test setup in the climate chamber had some limitations. For a better interpretation of the experimental results, it is important to discuss these issues.
The first issue is related to the long duration of the experiment. It took around 12 days for the saturated calcium silicate sample to completely dry out. During this time the conditions in the climate chamber could be affected by the outside climate conditions. Although the climate chamber was well insulated it could not be avoided that small heat gains or losses still occurred through the chamber walls. To reduce these gains or losses a second chamber was built around the climate chamber but even then small temperature fluctuations were noticed inside the chamber caused by long term fluctuations of the outside climate such as day-night fluctuations and weather fluctuations. These

temperature variations introduced an extra uncertainty in the measurements on top of the sensor uncertainty after calibration. To estimate this uncertainty, the drying experiment was repeated six times.
A second drawback of the climate chamber is the round air inlet. Contrary to a rectangular air inlet, which introduces a 2D air flow if the minimum height to width ratio is 7 [26], the round air inlet complicated the estimation of the convective boundary conditions at the top of the calcium silicate sample. The airflow over the calcium silicate surface has a three-dimensional character and by consequence the heat and mass transfer coefficient distribution over the surface is two-dimensional. This is more difficult to measure and to model than a 2D air flow. Nevertheless it is possible to estimate these transfer coefficients by using CFD (section 3.2).

2.4. Measurement results

As mentioned earlier both the mass change of the sample and the temperature at various depths in the sample were continuously registered during the experiment. Figure 4 shows the evolution of the sample mass during the first 9 days of the experiment.

Because boundary conditions during the test could vary due to the imperfect insulation of the climate chamber, measurements were performed six times to assess the impact of the boundary conditions. An average mass loss curve was derived from these measurements. The error bars indicate two times the standard deviation of the successive measurements and are a measure of the uncertainty on the mass loss due to variations in the boundary conditions between the experiments.

Two drying phases can be clearly distinguished from Figure 4: the first two days the sample mass decreases at a constant rate, which corresponds to the constant drying rate period (CRP). After 2 days the mass change slows down and the drying rate decreases. This is the start of the second drying period or falling rate period (FRP).

The measured temperature evolution in the calcium silicate during the first 9 days of the drying experiment is shown in Figure 5. Figures 5 a to d respectively show the temperature course at 7mm and 17mm depth in the calcium silicate sample (centre thermocouple), the temperature course at the bottom of the calcium silicate sample and the temperature course at the bottom of the insulation. The location of the thermocouples is shown in Figure 2.

In the temperature measurements, three drying stages can be clearly distinguished. During the constant drying period the temperature in the calcium silicate drops close to the wet bulb temperature. Due to heat gains through the insulated sample walls and by radiation from the surroundings, the temperature during the constant drying period is higher than the wet bulb temperature. The temperature courses in Figure 5 show a constant drying rate period for the first two days. This was also observed in the average moisture content measurements (Figure 4). After two days, when the surface of the calcium silicate sample starts to dry, the calcium silicate enters the second drying period (FRP). The drying rate decreases and the temperature in the calcium silicate sample rises: this can be clearly observed in Figure 5. Moreover, this temperature rise seems to occur in two phases: first the temperature rises to ± 24 °C, where a new temperature equilibrium occurs. After a while this temperature increases further, eventually to reach the supply air temperature when the sample is completely dried (i.e. 30°C ± 0.1°C).
A similar intermediate plateau in the temperature distribution during the falling rate period was also noticed by Kowalski et al during their drying experiments, in which they have studied the convective drying of a cylindrical sample made of kaolin (radius 0.03m and height 0.06m) [27]. The temperature distribution was determined by temperature probes inside the sample, drying curves were determined by weighing of the sample.
Since air flow approaches from one side of the sample, a boundary layer develops over the sample. Thermocouples were installed upstream and downstream of the central thermocouples.

Measurements from these thermocouples however showed that there was no significant leading edge effect. The measured temperatures in the sample during the drying experiment showed that the sample dried evenly. The observations will be further discussed by comparing them with simulation results.

3. Modelling convective drying of calcium silicate

In this section, the convective drying of calcium silicate sample will be studied more in detail by means of recently developed heat and moisture transport model that has been implemented into a 3D finite element solver (Fluent®).

3.1. Simulation model

A recently developed coupled heat and moisture transfer model including both vapour and liquid moisture transfer was used to study the specific drying course of the calcium silicate sample. An existing coupled CFD-HAM model including only vapour transfer [24,28] was adjusted and extended with liquid moisture transfer, so that phenomena such as drying of building materials could be studied more accurately.

In this section only a short description of the model is given. More details on the model can be found in [29,30]. The model has already been validated against a drying experiment from literature [12] in which ceramic brick was used as a hygroscopic and capillary active material. In the experiment, air was drawn through a wind tunnel and over a ceramic brick sample.

The model uses the gradient in capillary pressure p_c [Pa] as driving force for the liquid transport and the partial vapour pressure p_v [Pa] as driving force for the vapour transport. The moisture balance in a porous material is given by Eq. 1.

$$\frac{\partial w}{\partial t} = \nabla \cdot (\vec{g}_v + \vec{g}_l) = \nabla \cdot \left(\frac{D_{va}}{\mu R_v T} \nabla p_v + K_l \nabla p_c \right) \tag{1}$$

In Eq. 1 g_v and g_l are respectively the vapour and liquid flux [kg/s]. Eq. 1 is transformed to Eq. 2 using Kelvin's law and the relationship between relative humidity and partial vapour pressure ($RH = p_v/p_{sat}$) so that only temperature and capillary pressure remain as state variables.

$$\frac{\partial w}{\partial p_c}\frac{\partial p_c}{\partial t} = \nabla \cdot (\mathrm{K}_l \nabla \mathrm{p}_c) + \nabla \cdot \frac{D_{va}}{\mu R_v T}\left(\frac{\rho_v}{\rho_l} \nabla \mathrm{p}_c + RH \frac{\partial p_{sat}}{\partial T} \nabla \mathrm{T} - \frac{p_v \ln RH}{T} \nabla T \right) \tag{2}$$

In these equations p_{sat} is the saturation vapour pressure [Pa], K_l is the liquid permeability [s], w is the moisture content in the porous material [kg/m³], D_{va} [m²/s] is the diffusivity of water vapour into air, R_v the specific gas constant for water vapour [J/kgK] and T is the temperature [K]. μ is the vapour diffusion resistance factor: it is the ratio of the vapour diffusion of water vapour in the porous material to the vapour diffusion of water vapour in air. ρ_v and ρ_l are the vapour and liquid density [kg/m³] respectively.

The energy balance in the porous material states that a change in stored energy E [J] is due to heat conduction and transport of latent and sensible heat along with the moisture transport (Eq. 3).

$$\begin{aligned} &\frac{\partial E}{\partial t} = \frac{\partial}{\partial t}(\rho_{mat} h_{mat} + w_l h_l + w_v h_v) = \\ &(\rho_{mat} C_{mat} + w_l C_l + w_v C_v)\frac{\partial T}{\partial t} + C_l T \frac{\partial w_l}{\partial t} + (C_v T + L)\frac{\partial w_v}{\partial t} \\ &= \nabla \cdot (\lambda_{mat} \nabla T - C_l T g_l - (C_v T + L)\vec{g}_v) \end{aligned} \tag{3}$$

In Eq. 3 ρ_{mat} is the dry porous material density [kg/m³] and C_{mat} the heat capacity of the dry material [J/kgK]. w_v and w_l are the vapour and liquid moisture content respectively [kg/m³]. L is the latent heat of evaporation [J/kg].

3.2. Estimation of convective heat and mass transfer coefficients

In a building context, convective drying is the most important drying mechanism. Berger et al. [31] was able to study drying phenomena using a 1D finite difference model. The influence of various internal and external physical parameters was studied. Among others their study showed the impact of transfer coefficients on the drying rate. This model showed that the convective transfer coefficient determined the drying rate during the first drying rate period (the constant drying rate period). During the second drying rate period (the falling rate period) the drying rate is meanly determined by the internal transport properties of the porous material. Although 1D models already give a good insight in drying phenomena, studies showed that a correct representation of convective drying is only possible if 3D models are used. Boundary layers developing along the surface of a dried medium will result in a distributed drying rate across the mediums surface. Masmoudi et al. [32] showed that for convective drying this so called leading edge effect will be significant if the sample size is not clearly larger than the moisture and temperature boundary layer development zones. Several other researchers found similar conclusions [10,33-34].
For a representative simulation it is therefore important to include transfer coefficient distributions in the model. For the present case, the boundary condition for the calcium silicate top surface is complicated. As discussed earlier in this paper, due to the round air inlet of the climate chamber, the airflow over the calcium silicate sample has a 3-dimensional character and the convective heat and mass transfer coefficient distribution over the surface is 2-dimensional.

In order to estimate the convective transfer coefficients at the top of the sample preliminary CFD simulations were performed. In these simulations only the part near the inlet of the chamber was modelled. The temperature and mass fraction at the surface of the sample were kept constant. The inlet temperature was 30°C, the surface temperature of the calcium silicate sample was 20°C. The inlet mass fraction was 0,005226 kg/kg which corresponds with a relative humidity of 20%, the surface mass fraction was 0,01448 kg/kg. The measured inlet velocity profile depicted in Figure 3 was used as inlet conditions for the CFD simulation. The average turbulent intensity measured at the inlet was 3%.

Figure 6 shows the computational domain used for these simulations: a symmetric boundary condition is assumed for the middle plane of the inlet so only half of the inlet and test section is modelled. All external boundary faces were modelled as pressure outlets except the surface where the inlet is located. This plane was modelled as a wall. Only the flow, temperature and concentration field near the top surface of the calcium silicate have to be calculated exactly. Further from the calcium silicate surface the exact values are of less importance. The size of the domain can thus be limited to the area near the surface.
The SST k $-\omega$ model was used for turbulence modelling. Since the convective transfer coefficients have to be determined, a very fine grid is needed near the surface to make sure the boundary layers for velocity, heat and moisture are fully resolved. Therefore the y+ value should be around 1. The SIMPLE algorithm for pressure-velocity coupling was used. The convective terms where discretized with a second order upwind scheme. A double precision solver was used to reduce round off errors.

The grid independency was checked by comparing simulation results for a grid with 580800 cells with the results for a grid two times refined in every direction (8 times more cells). The average predicted heat and mass transfer coefficient, h and h_m, at the calcium silicate top surface were used for comparison. The difference between both predicted transfer coefficients was limited to 1%, hence it was concluded that the courser grid sufficed (table 1).

Figure 7 represents the predicted convective heat and mass transfer coefficients at the top surface of the calcium silicate sample only. Note that figure 7 is mirrored compared to the calculation domain as

depicted in Figure 6. The transfer coefficients are higher near the inlet where the boundary layer starts. A wake zone can be noticed in one corner of the calcium silicate surface, where recirculation occurs and the velocity and consequently the transfer coefficients are low. The wake zone is caused by the cylindrical inlet and the cylindrical form of the jet flowing over the calcium silicate surface. It is clear from this simulation that the transfer coefficients at the top surface have a complex distribution.

3.3. Simulations settings calcium silicate drying model

In order to simulate the actual drying of the calcium silicate sample, a computational domain representing the test setup was modelled (Figure 8). A grid with a total of 72390 cells was used. The grid was fine near the top surface and courser towards the bottom. The domain included the PUR insulation. Only half of the test sample is modelled since symmetry is assumed. The top surface consists of two parts: the CaSi surface and the PUR top surface. The PUR surface is assumed impermeable for moisture, a constant convective heat transfer coefficient of 25 W/m²K is imposed on this surface.
At the top surface of the calcium silicate sample, the preliminary predicted transfer coefficient distributions were imposed. The remaining PUR surfaces (sides and bottom) are all assumed impermeable for moisture and have a constant heat transfer coefficient of 8 W/m²K.
The simulated time was 9 days. Time steps of 60 seconds were taken, resulting in a total of 12960 time steps.

An additional radiation heat flux is added to the top surface to incorporate potential heat gains by radiation from the environment. The heat flux by radiation is calculated with Eq. 4. T_{roof} is the roof surface temperature of the climate chamber. The temperature of the surface is assumed to be 30°C. The emissivity of calcium silicate is estimated at 0.9 and that of the climate chamber wall (polyester lacquered, galvanized steel plate) is estimated at 0.9. The reference temperature was 30°C. The reference mass fraction was 0.005226kg/kg, corresponding with a relative humidity of 20%.

$$q_{rad} = \frac{C_b}{\frac{1}{\epsilon_1}+\frac{1}{\epsilon_2}-1}\left(T_{roof}^4 - T_s^4\right) \quad (4)$$

3.4. Material properties

Three material properties are needed in Eq 2: the vapour diffusion resistance factor μ, the liquid permeability K_l and the moisture capacity ∂w/∂pc.
The material properties of calcium silicate were measured extensively during the HAMSTAD project by KULeuven [16,35]. These properties were used as input for the CFD-HAM model. The properties of calcium silicate can be found in Table 2.

The water vapour resistance factor can be formulated by:

$$\mu = [0.33 + 2.49 \times 10^{-6} exp(6.84RH)]^{-1} \quad (5)$$

The sorption isotherm is written by Eq. 6, with a = -2.936 x 10^{-5} and n = 1.7266.

$$w = w_c\left[1 + \left(a\rho_{liq}R_vTln(RH)\right)^n\right]^{\frac{(1-n)}{n}} \quad (6)$$

The liquid permeability of calcium silicate is shown in Figure 9.

3.5. Validation

The drying experiment is simulated with the coupled heat and moisture transfer model. Figures 4 and 5 show, apart from the measurement results, also the results of the numerical simulation. A good agreement between the measurements and simulations was found both for the temperatures at

various depths in the calcium silicate sample as for the mass change of the sample. Thus the model is able to predict the convective drying of the calcium silicate sample over a long period.

The good correspondence of the measured and simulated constant rate period indicates that the heat and mass transfer coefficients at the surface are well-estimated, since in the first drying phase the rate of drying is almost entirely determined by the air side boundary conditions.
Also the onset of the falling rate period and the mass decrease during this second drying period is in good agreement with the measurements. During the falling rate period the moisture transport at the surface is dominated by vapour diffusion. During this period the hygric material properties determine the drying behaviour. Since the measurements and simulations correspond well, also during this drying period, it can be concluded that the material properties are accurate enough.

The simulations show the intermediate temperature plateau during the second drying period that was also observed in the measurements. In order to study this phenomenon more in detail, the temperature distribution in the sample was plotted every 24 hours in Figure 10. On the x-axis the length of the sample is shown, on the y-axis the height of the sample is presented. The PUR insulation layer is also depicted in Figure 10, the calcium silicate sample is indicated with a thin black line.
These simulations show how the low temperature zone moves into the material as the material dries. This can be seen in the temperature distribution after the first day of the simulation (Figure 10 a): the temperature at the top surface of the sample drops to about 16°C, while the bottom side still has a temperature of about 24°C. The moving moisture front in the material explains the observed intermediate temperature plateau. As the material dries out, a moisture front is formed and moves into the material. On one side of the moisture front the relative humidity is low, here the sample is dry, on the other side of the moisture front the relative humidity is high (close to 100%) since the sample is still wet there. Figure 11 depict this moving moisture front. In this figure the moisture content distribution along the depth of the sample is depicted. A graph is plotted for each day corresponding with the nine temperature distribution plots of Figure 10.
It is at the moisture front that liquid water evaporates. The vapour is then transported to the surface of the sample by diffusion. For the evaporation at the moisture front, energy is needed for the phase change. This latent heat change results in a local temperature drop at the moisture front. The intermediate temperature plateau is extra pronounced due to the low heat conductivity of the calcium silicate when dry. The dry top layer of the calcium silicate acts as an insulation layer on top of the wet material, keeping the temperature in the wet part of the calcium silicate sample low.
At the start of the experiment, when the sample is completely saturated with water, it has a moisture content of about 780-790 kg/m³. At that moment, the average thermal conductivity of the sample is about 0,5 W/mK. As the sample dries out, the moisture content decreases and correspondingly does the thermal conductivity. At the end of the first drying phase (day 2), the moisture content has decreased to about 250 kg/m³ (Figure 4), and the average thermal conductivity of the sample has dropped about 2,5 times, to about 0.2 W/mK. At the end of the experiment (day 9), the average thermal conductivity has decreased even further, to about 0.07 W/mK (corresponding to a moisture content of 20 kg/m³ of the calcium silicate sample).
This phenomenon is clearly linked to hygroscopic capillary insulation materials and is not found in non-insulating porous materials such as ceramic brick [12].

The temperature plateau that was observed in Figure 5 between the 2nd and 5th day of the drying experiment can also be noticed in Figure 10: during this period the temperature in the upper layer of the sample stayed more or less stable around 24°C, while from the 5th to the 7th day on, the temperature increased to about 28°C, which is in accordance with the findings from Figure 5.
Comparing this with Figure 11 shows that the temperature increase in Figure 5 starts as soon as the moisture front crosses the sample position.

It was mentioned in section 2.4 that no leading edge effect was observed in the measurements. The same counts for the simulations. This is in contrast to e.g. the drying experiment with brick [12,29-30]

that was used to validate the coupled heat and mass transfer model and the observation by [10,32-34]. This shows that the use of spatially varying transfer coefficients is not always needed and is very case specific and depends on the material properties, the geometry and 'intensity' of the transfer coefficient distribution. For example high thermal conductivity will result in an even temperature distribution in the sample. Since the sample is initially wet, thermal conductivity is high. High moisture permeability will result in an even moisture distribution in the sample, even if at one side drying rates are higher. Internally in the sample the moisture content will be continuously redistributed.
The effect of geometry is notices for example in a sample with sharp edges. Such a sample would experience much higher transfer coefficient at those edges and it is likely that their drying out of the sample would occur faster. The present sample had no such edges.
Finally the intensity of the transfer coefficient distribution effects temperature and moisture distribution in the sample. For example an impinging jet configuration would create very high transfer coefficient locally on the surface and would result in local temperature and moisture distributions. For a parallel flow over a plane surface the transfer coefficient distribution is less severe.

A distinction should be made between leading edge effect and the effect that edges have on the simulation results. The measurements and simulations indeed show that there is no leading edge effect. In other words, there is no effect of the developing boundary layer over the sample which results in a larger transfer coefficient for heat and mass at the leading edge of the sample than for the trailing edge. This is shown in the almost symmetrical temperature distributions in Figure 10. However the other boundaries or 'edges' do have a great effect on temperature distribution. Heat is transferred between the sample and the environment not only at the top but also at the sides and bottom, resulting in a 3D distribution of the temperature. Only a 3D model will be able to capture this effect. As a result the absence of a leading edge effect does not automatically imply that simple 1D or 2D modelling would suffice.

4. Conclusions

In this paper a convective drying experiment showed a specific drying course of a calcium silicate sample. The second drying stage or falling rate period showed an intermediate plateau in the temperature course. This plateau was explained by comparing the measurements with simulation results. A newly developed heat and moisture transport model was used for these simulations. The model includes coupled heat and moisture transport in porous materials for both water vapour diffusion and liquid water transport. This makes the model specifically suitable for the simulation of drying phenomena.
By comparing the measurements with the simulations, it was shown that the temperature plateau during the falling rate period was caused by the high insulation value of dry calcium silicate. As a moisture front moves into the calcium silicate during drying, a zone of lower temperature moves along with the front. The dry calcium silicate above the moisture front acts as insulation layer so that heat needed for the evaporation of liquid water at the moisture front, is taken from the sample, thus locally lowering the sample temperature.
Finally, the drying of the calcium silicate sample did not show any leading edge effect, in contrast to what other researchers found for other materials (such as e.g. brick). This emphasizes that the importance of using spatially varying transfer coefficients is very much case dependent.

5. Acknowledgements

The results presented in this paper were obtained within the frame of the research project IWT-SB/81322/Van Belleghem funded by the Flemish Institute for the Promotion and Innovation by Science and Technology in Flanders and the IWT SBO-050451 project Heat, Air and Moisture Performance Engineering: A Whole Building Approach. Their financial support is gratefully acknowledged.
Special thanks go to Prof. Staf Roels from KULeuven who provided the CaSi samples and prof. Hans Janssen for the fruitful discussions on the model development.

Finally the authors wish to tank Wout De Geyter and Giovanni Stuer for their help and contribution to the experimental results.

6. References

[1] M. S. Al-Hamoud. Performance characteristics and practical applications of common building thermal insulation materials. Build Environ 40(3):353-366, 2005

[2]A. Abdou, I. Budaiwi. The variation of thermal conductivity of fibrous insulation materials under different levels of moisture content. Constr Build Mater 43: 533-544, 2013

[3] E. Vereecken and S. Roels. Review of mould prediction models and their influence on mould risk evaluation. Build Environ 51(0):296-310, 2012.

[4] A. Nicolai. Modeling and numerical simulation of salt transport and phase transitions in unsaturated porous building materials. Phd thesis, Syracuse University, USA 2008.

[5] T.D. Goncalves, L. Pel, J.D. Rodrigues. Influence of paints on drying and salt distribution processes in porous building materials. Constr Build Mater 23(5): 1751-1759, 2009

[6] A.S. Mujumdar. Handboek of Industrial Drying. CRC Press, 3th edition, 2007.

[7] O. Krischer. Die wissenschafftlichen Grundlagen der Trochnungstechnik. Springer-Verlag, Berlin/Göttingen/Heidelberg, 2th edition, 1963.

[8] L. S. Oliveira and K. Haghighi. Conjugate heat and mass transfer in convective drying of porous media. Numer Heat Tr A - Appl 34(2):105-117, 1998.

[9] T. Defraeye, G. Houvenaghel, J. Carmeliet and D. Derome. Numerical analysis of convective drying of gypsum boards. Int J Heat Mass Tran 55(9-10):2590-2600, 2012

[10] H. Shokouhmand, V. Abdollahi, S. Hosseini, and K. Vahidkhah. Performance Optimization of a Brick Dryer Using Porous Simulation Approach. Dry Technol 29(3):360-370, 2011

[11] K. Murugesan, H. N. Suresh, K. N. Seetharamu, P. A. A. Narayana and T. Sundararajan. A theoretical model of brick drying as a conjugate problem. Int J Heat Mass Tran 44(21):4075-4086, 2001

[12] T. Defraeye. Convective Heat and Mass Transfer at Exterior Building Surfaces. Phd. thesis, KULeuven, Belgium 2011.

[13] J. D. Mar, E. Litovsky and J. Kleiman. Modeling and database development of conductive and apparent thermal conductivity of moist insulation materials. J Build Phys 32(1):9-31, 2008

[14] Z. Pavlík, J. Mihulka, L. Fiala and R. Cerný. Application of Time-Domain Reflectometry for Measurement of Moisture Profiles in a Drying Experiment. Int J Thermophys 33:1661-1673, 2012

[15] Calsitherm. http://www.calsitherm.de/en/products.htm

[16] S. Roels, J. Carmeliet and H. Hens. HAMSTAD WP1 - Moisture transport properties and material characterisation - Final report. Technical report, KULeuven, 2003.

[17] A. Hamilton, and C. Hall. Physicochemical Characterization of a Hydrated Calcium Silicate Board Material, J Build Phys 29(1):9–19, 2005

[18] C.T. Do, D.p. Bentz and P. E. Stutzman. Microstructure and thermal conductivity of hydrated calcium silicate board materials. J Build Phys 31(1):55-67, 2007

[19] J. Carmeliet, S. Roels. Determination of the moisture capacity of porous building materials. J Build Phys 25(3):209-237, 2002

[20] B. J. Pease, G. A. Scheffler and H. Janssen. Monitoring moisture movements in building materials using X-ray attenuation: influence of beam-hardening of polychromatic X-ray photon beams. Constr Build Mater 36:419-429, 2012

[21] J. Xu and J. S. Zhang. An experimental study of relative humidity effect on VOC's effective diffusion coefficient and partition coefficient in a porous medium. Build Environ 46(8):1785-1796, 2011

[22] M. Steeman, M. Van Belleghem, M. De Paepe and A. Janssens. Experimental validation and sensitivity analysis of a coupled BES-HAM model. Build Environ, 45(10):2202-2217, 2010.

[23] M. Van Belleghem, M. Steeman, A. Willockx, A. Janssens and M. De Paepe. Benchmark experiments for moisture transfer modelling in air and porous materials. Build Environ, 46(4):884-898, 2011.
[24] H.-J. Steeman, M. Van Belleghem, A. Janssens and M. De Paepe. Coupled simulation of heat and moisture transport in air and porous materials for the assessment of moisture related damage. Build Environ 44(10):2176-2184, 2009.
[25] M. Steeman, A. Janssens, H.-J. Steeman, M. Van Belleghem and M. De Paepe. On coupling 1D non-isothermal heat and mass transfer in porous materials with a multizone building energy simulation model. Build Environ 45(4):865-877, 2010.
[26] R. B. Dean. Reynolds Number Dependence of Skin Friction and Other Bulk Flow Variables in Two-Dimensional Rectangular Duct Flow. J Fluids Eng 100(2):215-233, 1978.
[27] S.J. Kowalski, G. Musielak and J. Banaszak. Experimental validation of the heat and mass transfer model for convective drying. Dry Technol 25:107-121. 2007.
[28] M. Van Belleghem, H.-J. Steeman, M. Steeman, A. Janssens, and M. De Paepe. Sensitivity analysis of CFD coupled non-isothermal heat and moisture modelling. Build Environ, 45(11):2485-2496, 2010.
[29] M. Van Belleghem, M. Steeman, H. Janssen, A. Janssens and M. De Paepe. Validation of a coupled heat and moisture transport model for porous materials integrated in CFD. Submitted to Int J Heat Mass Tran.
[30] M. Van Belleghem. Modelling coupled heat and moisture transfer between air and porous materials for building applications. PhD thesis. Ghent University, Belgium, 2013.
[31] D. Berger and D. C. T. Pei. Drying of hygroscopic capillary porous solids - a theoretical approach," Int J Heat Mass Tran 16:293-302, 1973.
[32] W. Masmoudi and M. Prat. Heat and Mass-Transfer between a Porous-Medium and a Parallel External Flow - Application to Drying of Capillary Porous Materials. Int J Heat Mass Tran 34(8):1975-1989, 1991.
[33] A. Kaya, O. AydIn and I. Dincer. Numerical modeling of heat and mass transfer during forced convection drying of rectangular moist objects. Int J Heat Mass Tran 49(17-18):3094-3103, 2006.
[34] V.P.C. Mohan and P. Talukdar. Three dimensional numerical modeling of simultaneous heat and moisture transfer in a moist object subjected to convective drying. Int J Heat Mass Tran, 53(21-22):4638-4650, 2010.
[35] O. Adan, H. Brocken, J. Carmeliet, H. Hens, S. Roels and C.-E. Hagentoft. Determination of Liquid Water Transfer Properties of Porous Building Materials and Development of Numerical Assessment Methods: Introduction to the EC HAMSTAD Project. J Build Phys, 27(4):253–260, 2004.

Figure 1. Schematic representation (vertical section) of the climate chamber with the calcium silicate test sample placed on top of a balance.

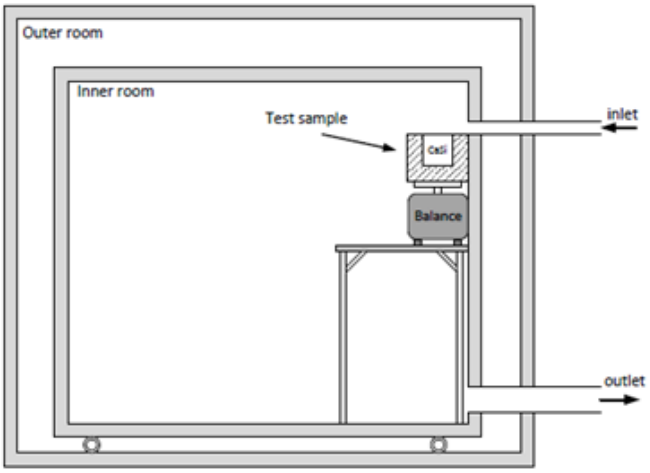

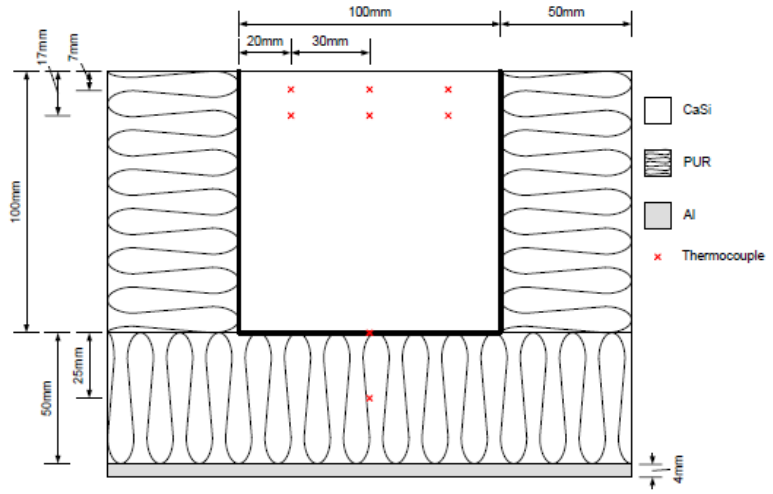

(a) Longitudinal section test sample

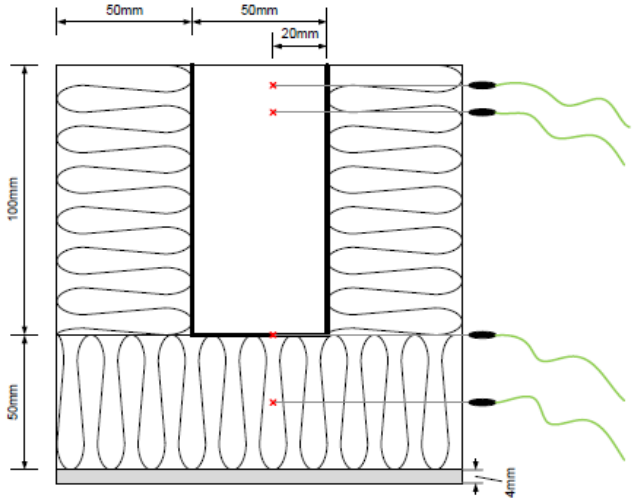

(b) Cross section test sample

Figure 2. Schematic representation of the longitudinal (a) and cross section (b) of the test sample for the drying experiment (CaSi = calcium silicate, PUR = polyurethane, Al = aluminium)

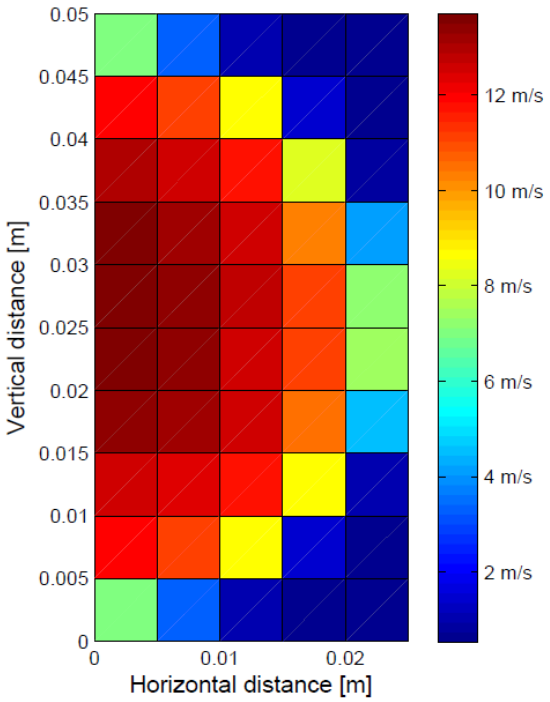

Figure 3. Velocity profile at the inlet of the climate chamber showing a grid of discrete measurement points, coloured according to the measured speed in the centre of a square.

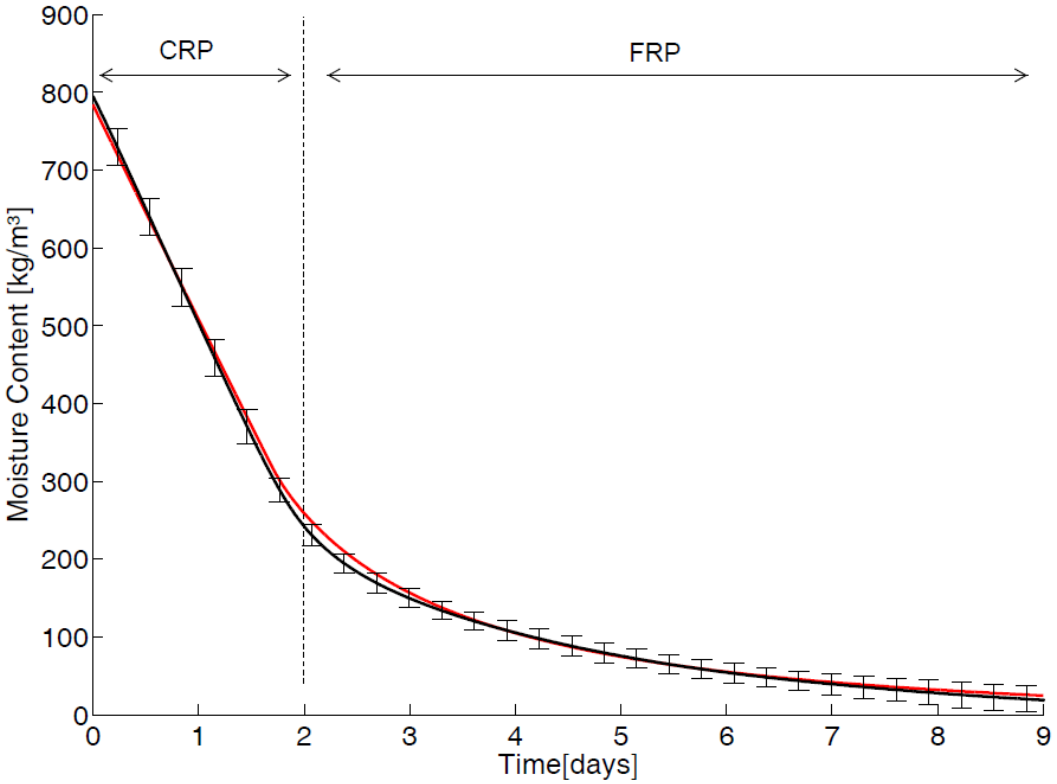

Figure 4. Measured (black) an simulated (red) moisture content the calcium silicate sample with indication of the constant rate period (CRP) and the falling rate period (FRP).

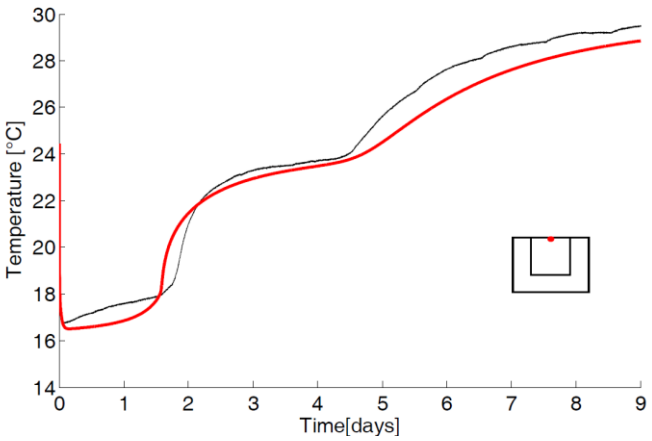

(a)Temperature at 7mm depth in the calcium silicate sample

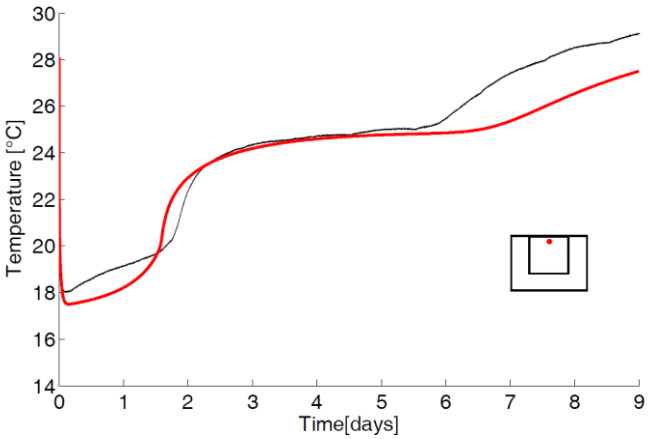

(b)Temperature at 17mm depth in the calcium silicate sample

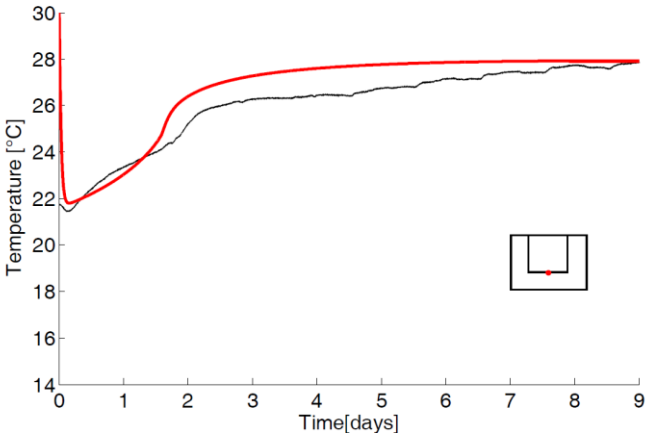

(c)Temperature at the bottom of the calcium silicate sample

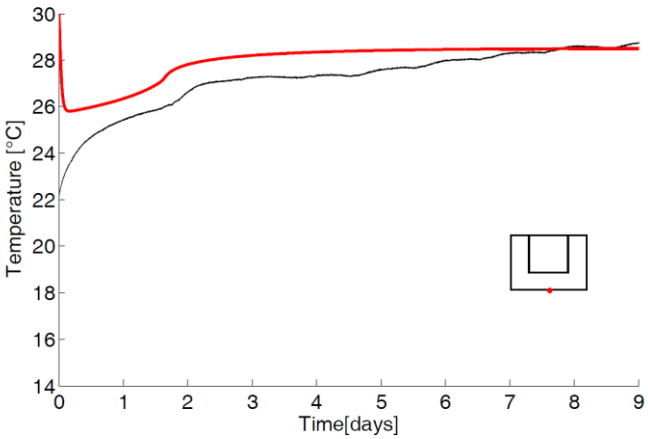

(d)Temperature at the bottom of the PUR insulation

Figure 5. Temperature measurements (black) and simulated (red) temperatures at different positions in the sample at a depth of 7mm (a) and 17mm (b) in the calcium silicate sample and at the bottom of the sample (c) and below the insulation (d).

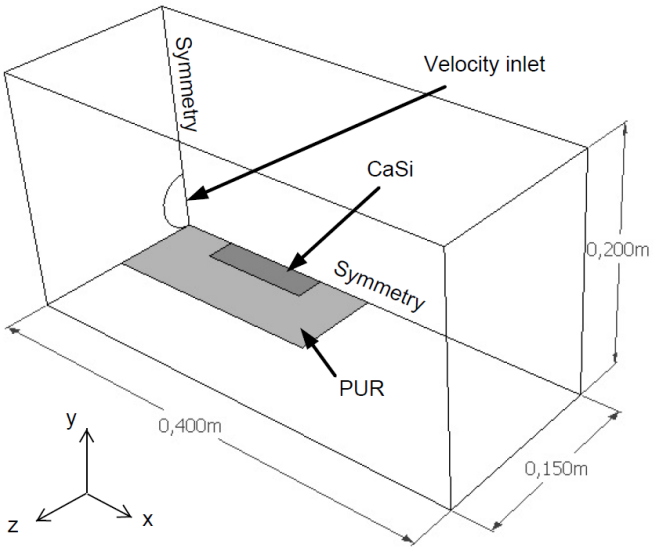

Figure 6. Schematic representation of the part of the climate chamber used to simulate the air flow over the top of the sample (dark grey: CaSi top surface, light gray: PUR surface)

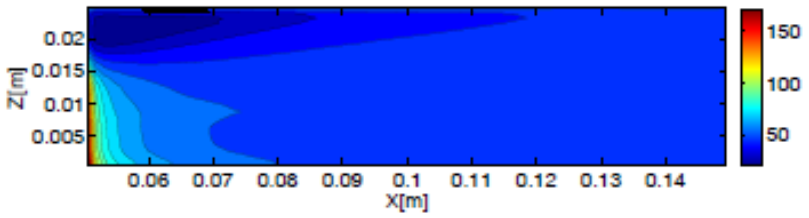

(a) CHTC

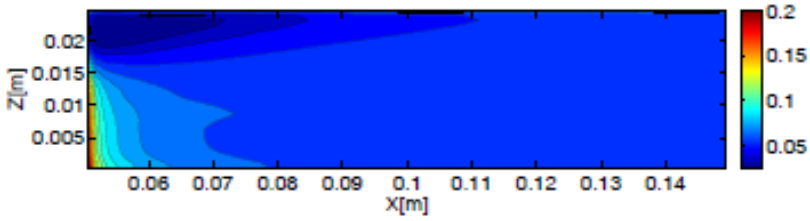

(b) CMTC

Figure 7. Distribution of the convective heat transfer coefficient in W/m²K (a) and the convective mass transfer coefficient in s/m (b) at the surface of the CaSi sample

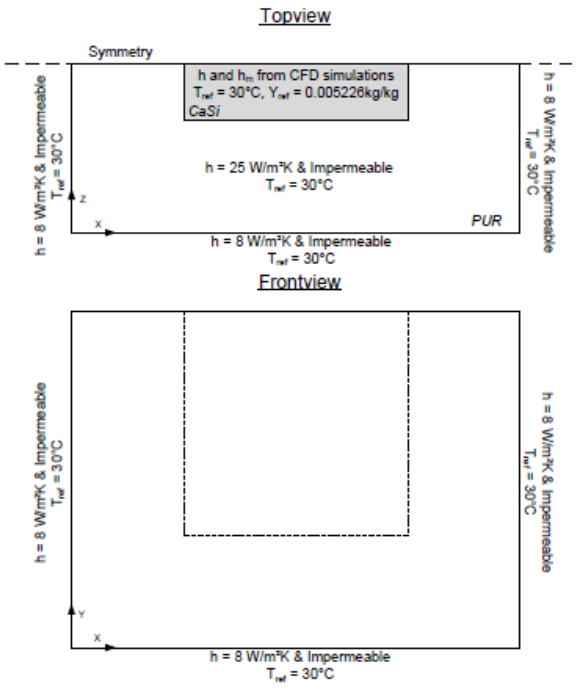

Figure 8. Computational model for CaSi sample: boundary conditions on exterior surfaces

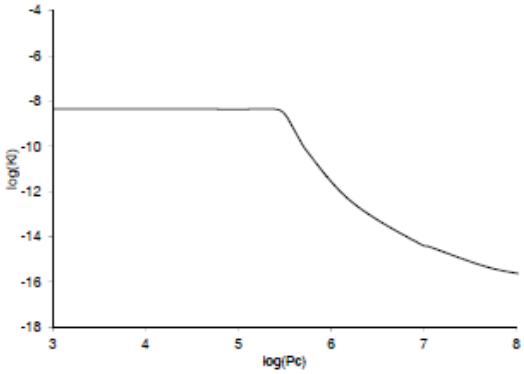

Figure 9. Liquid permeability of calcium silicate, based on [16,35]

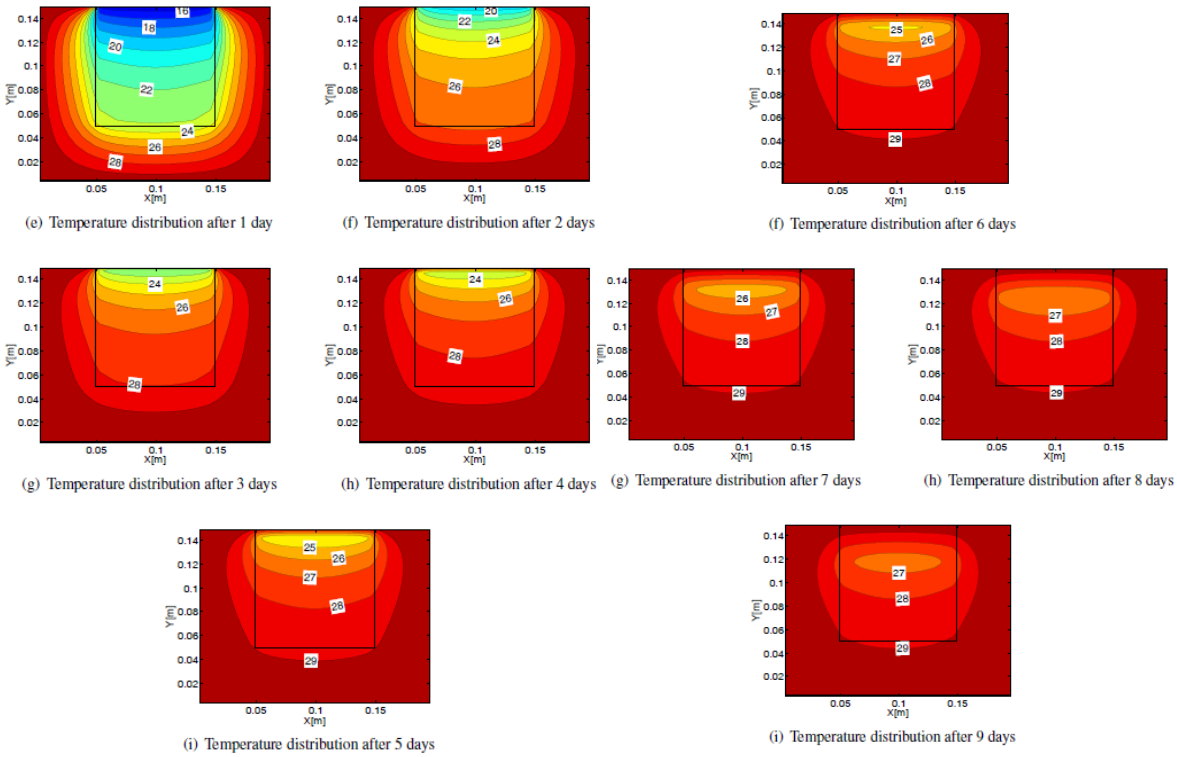

Figure 10 Temperature distribution in a longitudinal section of the calcium silicate sample, every 24 hours

Table 1. Average heat and mass convective transfer coefficients for a course and more dense grid.

	580800 cells	**4646400 cells**	**Difference**
h	50.3	50.8	1%
h_m	0.0597	0.0603	1%

Table 2. Material properties of calcium silicate [6,21]

Density ρ [kg/m³]	270
Heat conduction coefficient λ [W/mK] as function of moisture content w [kg/m³]	$0.06+5.6 \times 10^{-4}$ w
Specific heat c_p [J/kgK]	1000
Vapour resistance μ_{dry} [-]	3
Capillary moisture content w_c [kg/m³]	894
Open porosity ψ_0 [-]	0.894